LANGMUIR Article
Cite This: Langmuir 2019, 35, 13915−13922
pubs.acs.org/Langmuir

Photothermal Actuation of Diverse Liquids on an Fe_3O_4-Doped Slippery Surface for Electric Switching and Cell Culture

Sizhu Wu,[†] Lili Zhou,[†] Chao Chen,*[,§] Lu-An Shi,[∥] Suwan Zhu,[§] Chengchu Zhang,[‡] Dong Meng,[†] Zhouchen Huang,[§] Jiawen Li,[§] Yanlei Hu,[§] and Dong Wu*[,§]

[†]School of Instrument Science and Optoelectronics Engineering and [‡]Institute of Industry and Equipment Technology, Hefei University of Technology, Hefei 230009, China

[§]CAS Key Laboratory of Mechanical Behavior and Design of Materials, Department of Precision Machinery and Precision Instrumentation, Key Laboratory of Precision Scientific Instrumentation of Anhui Higher Education Institutes and [∥]CAS Center of Excellence in Nanoscience, Hefei Science Center of CAS, Department of Chemistry, University of Science and Technology of China, Hefei 230026, China

Supporting Information

ABSTRACT: The photoinduced manipulation of liquids on a slippery lubricant-infused porous surface (SLIPS) has attracted a tremendous amount of attention because of its merits of contactless stimulation and excellent spatial and temporal control. However, tedious fabrication methods by a combination of template transfer and fluorination for a photothermal-material-doped SLIPS and the lack of deeper systematically quantitative analysis with respect to droplet hydrokinetics are greatly perplexing in both academic research and industrial applications. Here we demonstrate a kind of Fe_3O_4-doped SLIPS by one-step femtosecond laser cross-scanning, which can readily steer diverse liquids toward arbitrary directions with a fast velocity of up to 1.15 mm/s in the presence of a unilateral NIR stimulus. The underlying mechanism is that the wettability gradient force ($F_{wet\text{-}grad}$) induced by the temperature gradient arising from asymmetric near-infrared-irradiation (NIR) loading would be generated within 1 s to actuate a targeted droplet's sliding behavior. Through tuning the NIR irradiating sites, we can slide a targeted droplet with controllable directions and routes. On the basis of fundamental physics, we have quantitatively analyzed the relationship among Fe_3O_4-doped content, lubricant rheological performance, droplet wettability variations, $F_{wet\text{-}grad}$, and the sliding velocity for diverse liquid species. Accordingly, we can remotely steer liquid droplets to realize the on−off state of an electrical circuit on demand, the droplet fusion of a microfluidic reactor, and the culture/inhibition of biological cells.

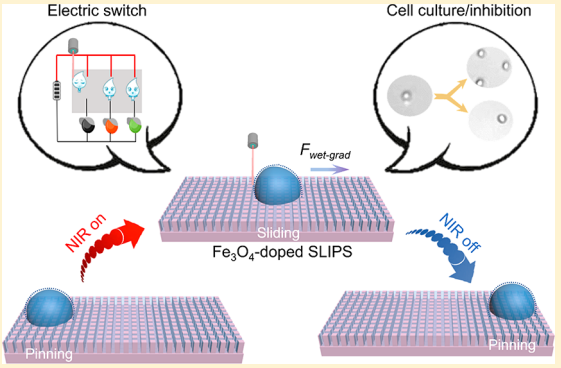

INTRODUCTION

In the past decade, smart surfaces for droplet motion control have aroused considerable research interest on account of their tremendous potential in both scientific investigations and industrial applications, including droplet-relevant microfluidics,[1,2] "no-loss" droplet transport,[3,4] two-phase oil−water separation,[5,6] biotechnology,[7,8] self-cleaning,[9−11] anti-icing,[12,13] and so on. Accordingly, a variety of methods have been deployed by means of physicochemical,[14−17] thermal,[18,19] electrical,[20,21] magnetic,[22,23] and photoinduced[24,25] platforms. Among these external stimuli, by taking advantage of remote, contactless, and low-contact-angle hysteresis merits, a photoinduced slippery surface is a competitive alternative.[26] In general, the doped photoresponsive additives (e.g., graphene and Fe_3O_4) impart the new surface with photothermal functionality for the introduction of a giant wettability gradient force ($F_{wet\text{-}grad}$). Meanwhile, the infused lubricants render the new surface with an air/liquid/liquid/solid (ALLS) system for steering microdroplets with ease. For example, Wang et al.[27] demonstrated a state-of-the-art property in programmable wettability by utilizing a paraffin-infused porous graphene film (PIPGF), which had provided a paradigm of achieving the controllable sliding pathways for liquid droplets through the dynamic and reversible transition between a liquid and a solid surface in response to near-infrared (NIR) light irradiation. Although this work has greatly advanced the impetus in realizing the spatiotemporal droplet manipulation by flexibly changing the NIR masks, the high hysteresis resistance of paraffin still hinders its manipulation ability. In this regard, Gao et al.[26] developed a kind of Fe_3O_4-doped slippery photoresponsive organogel surface (POS) for highly efficient droplet transport by utilizing a synergistic effect between the droplet asymmetrical deformation and the inside Marangoni flows, which had been derived from an NIR-induced dynamic temperature gradient (ΔT) and a further $F_{wet\text{-}grad}$. Although controllable sliding routes and velocities have been demon-

Received: July 5, 2019
Revised: September 12, 2019
Published: September 30, 2019

DOI: 10.1021/acs.langmuir.9b02068
Langmuir 2019, 35, 13915−13922

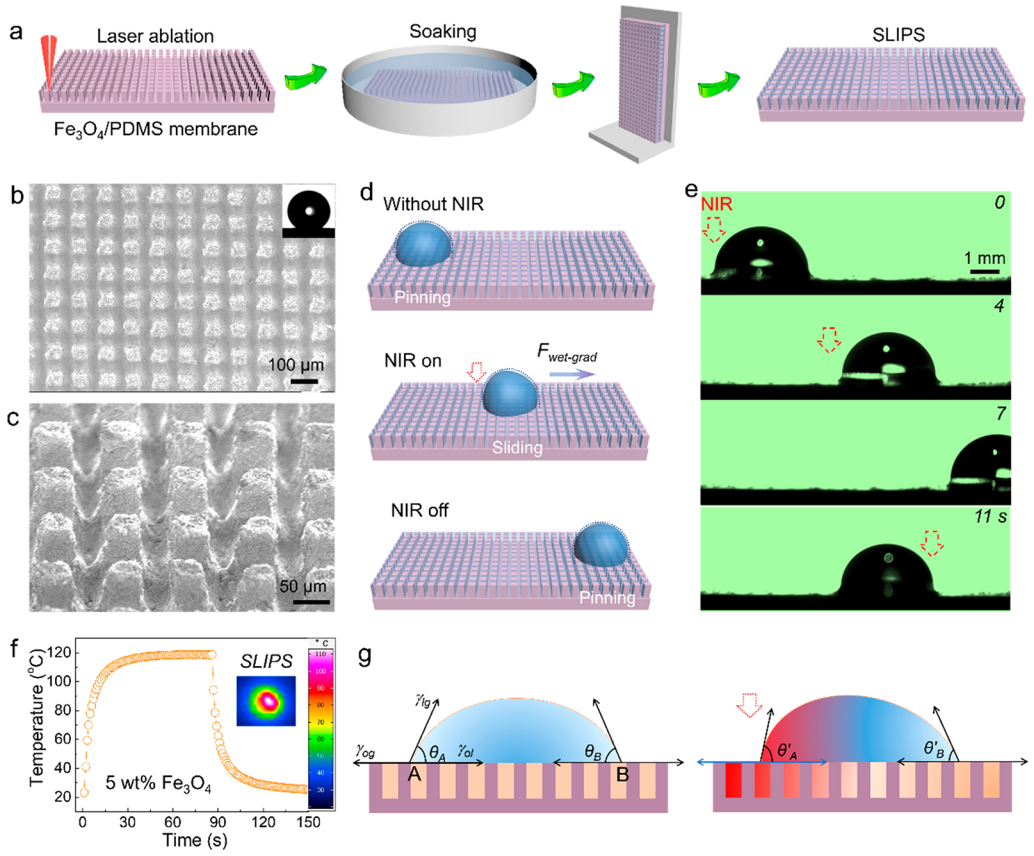

Figure 1. Facile fabrication of Fe_3O_4-doped SLIPS. (a) Schematic diagram for the fabrication strategy composed of one-step femtosecond laser cross-scanning, soaking, and fast removal of the residual lubricant oil. SEM images of the (b) top and (c) sectional view for the as-prepared PAF by femtosecond laser cross-scanning. (d) Schematic diagram for droplet motion control between pinning and sliding on NIR-responsive SLIPS. (e) Digital clips for demonstrating the controllable droplet's moving directions by tuning the NIR irradiating sites. (f) Temperature−time curve for NIR-irradiated SLIPS (Fe_3O_4-doped content, 5 wt %; distance between NIR and SLIPS, 7 cm). (g) Mechanism illustration of the wettability gradient variation without/with a unilateral NIR stimulus.

strated in the above method, several obstructions are still somewhat puzzling: (1) As the prerequisite for preventing the intrusion of targeted liquids floating above a repellent lubricant oil, a superhydrophobic porous substrate has been harvested by a combination of the template-transfer method and chemical fluorination, which is tedious and not environmentally benign. (2) Though numerous forces including $F_{wet\text{-}grad}$, Marangoni force (F_M) and hydrodynamic resistance (F_H) have been mentioned, and the quantitative relationship among lubricant rheological parameters (viscosity and surface tension), $F_{wet\text{-}grad}$, and the sliding velocity for diverse liquids has not been examined. Therefore, there is a need to deploy a more facile and environmentally friendly method for a porous photothermal material-based slippery surface and to give deep insight into the underlying mechanism in terms of hydrodynamic quantitative analysis.

Herein, we prepare a kind of Fe_3O_4-doped SLIPS by one-step femtosecond laser cross-scanning, which can easily manipulate diverse liquids in arbitrary directions at speed as high as 1.15 mm/s in the presence of a unilateral NIR stimulus. The underlying mechanism is that $F_{wet\text{-}grad}$ induced by the apparently asymmetric NIR loading, which indeed originates from a temperature gradient and another Laplace pressure difference at the two ends of the droplet, would be generated within 1 s to actuate a targeted droplet's sliding behavior. Once the NIR stimulus was discharged, the vanishing of $F_{wet\text{-}grad}$ depending on heat transfer and conversion tends to brake the droplet instantly. Through modulating the NIR sites, we can slide a targeted droplet with controllable directions and routes. On the basis of fundamental physics, we have quantitatively analyzed the relationship among Fe_3O_4-doped content, lubricant rheological performance, droplet wettability variations, $F_{wet\text{-}grad}$, and sliding velocity for diverse liquid species. More significantly, we can remotely steer liquid droplets to realize the on−off state of an electrical circuit on demand, droplet fusion of a microfluidic reactor, and culture/inhibition of biological cells. This work provides insight into the design of *Nepenthes*-inspired light-responsive materials for droplet manipulation, which would further benefit researchers engaged in biomedical engineering, laboratory-on-a-chip, microfluidics, microengines, and so on.

METHODS

Experimental Section. *Materials.* PDMS Sylgard 184 used as the host matrix was purchased from Dow Corning (Auburn, MI). Fe_3O_4NPs (10 nm, 99.9% purity) was purchased from Kelly Institute of Metallurgy (Tianjin, China). Silicone oil (1, 5, 10, and 100 cSt), liquid paraffin, castor oil, ethanol, ethylene glycol, and glycerol were purchased from Ruisi Reagent (Chengdu, China) and used without further purification. Glucose powder, indigo carmine powder, sodium chloride powder, and sodium hydroxide powder were purchased from Aisiwei Microbial Culture Medium (Hangzhou, China). Potassium sorbate (98% purity) was purchased from BOMEI Experimental Market (Hefei, China). Dry yeast was purchased from Angel Yeast Co., Ltd. (Shanghai, China).

DOI: 10.1021/acs.langmuir.9b02068
Langmuir 2019, 35, 13915−13922

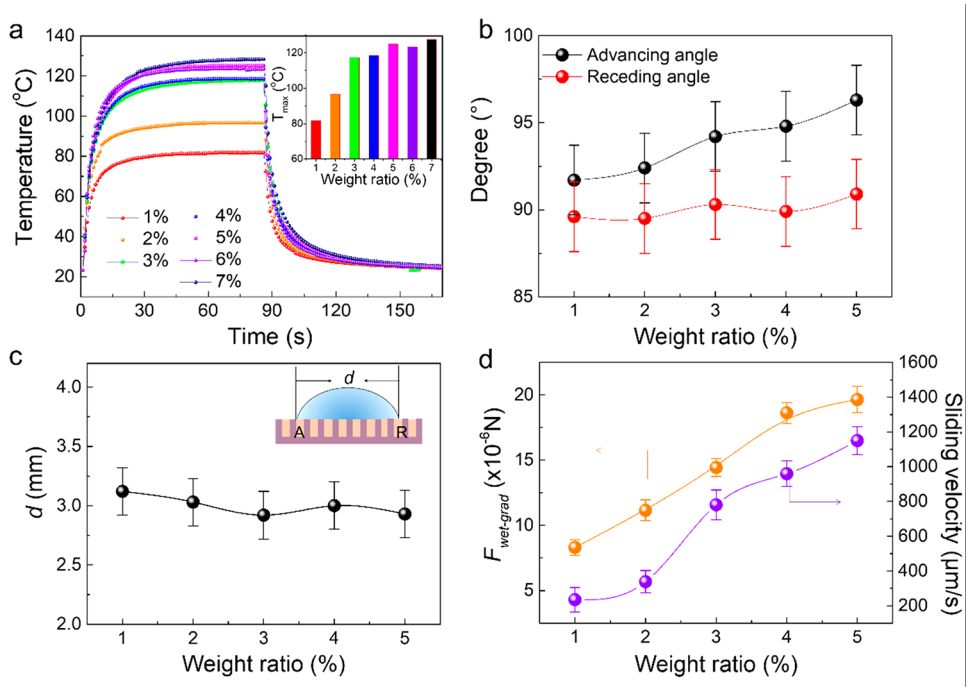

Figure 2. Effect of Fe_3O_4-doped content on droplet hydrodynamics. (a) Time-dependent temperature profiles for NIR-irradiated SLIPS with different Fe_3O_4-doped contents. Corresponding variations of a droplet's (10 μL) (b) θ_A and θ_R, (c) characteristic length, and (d) $F_{wet\text{-}grad}$ and average sliding velocity as a function of Fe_3O_4-doped content.

NIR Light Source. An 808 nm NIR laser (300 mW power, 2.3 × 1.4 mm^2 spot area) was purchased from Standing Laser (Shenzhen, China). The irradiation distance of NIR could be adjusted in the range of 10−50 cm by a homemade holder. In this work, the irradiation distance of NIR was set as 10 cm.

Preparation of a PDMS/Fe_3O_4 Glue Composite. First, Fe_3O_4 nanoparticles, a PDMS prepolymer, and a PDMS curing agent (10:1 ratio of the base and curing agent) were mixed together by stirring manually and then mechanically mixed for 5 min at 2000 rpm. Second, the homogeneous mixture was poured onto a Petri dish and placed in a vacuum chamber for 1 h to remove air bubbles, followed by curing at 100 °C for 30 min. Finally, the cured Fe_3O_4/PDMS composites were carefully peeled off of the Petri dish.

Femtosecond Laser Fabrication. The 3D micropillar structures on the sample were achieved by cross scanning. The laser beam (104 fs, 1 kHz, 800 nm) from a regenerative amplified Ti:sapphire femtosecond laser system (Legend Elite-1K-HE, Coherent, USA) was employed for ablation. The laser power, scanning spacing, and speed were set at 250 mW, 100 μm, and 4 mm s^{-1}, respectively.

Yeast Culture and Inhibition. The liquid culture medium was produced by sterilizing the mixture of solid granular Sabouraud's glucose broth medium (10.0 g L^{-1} peptone, 40 g L^{-1} glucose, pH 5.6 ± 0.2 at 25 °C, QingDao Hope Biotechnology CO., Ltd.) and distilled water with a concentration of 50 g L^{-1} at 120 °C for 20 min. The liquid cytostatic was produced by dissolving 5.4 g of potassium sorbate into 8 mL of distilled water. The yeast solution was produced by dissolving a grain of dry yeast uniformly into 3 mL of distilled water.

Characterization. The surface structures of SLIPS were observed by field emission scanning electron microscopy (JSM-7500F, JEOL, Japan) at 5 kV. The contact angles (CAs) of droplets on samples were measured by an OCA 20 contact angle meter system (Dataphysics Instruments GmbH, Germany) at ambient temperature. Deionized water (5.0 μL) was dropped onto the samples, and the static CA was determined by the average of at least five measurements. The infrared thermal images of irradiated SLIPS under NIR were visualized with an infrared thermometer (VarioCAMhr head 680, InfraTec). The chemical composition was analyzed by X-ray diffraction (XRD) patterns (D/MAX2500 V, Japanese Neo-Confucianism Manufacturing, Japan). High-magnification movies for steering diverse microdroplets were captured by the contact angle meter equipped with ScreenCAP software (bandicam) with a resolution of 1280 × 1024. Videos for displaying the current light-responsive SLIPS's potential applications in the cell culture and the electric switch were captured with a mobile phone (iPhone 8) at a resolution of 1920 × 1080.

RESULTS AND DISCUSSION

Facile Fabrication of SLIPS and Its Characterization. The fabricating strategy of smart SLIPS was composed of femtosecond laser cross-scanning for a superhydrophobic micropillar-arrayed Fe_3O_4/PDMS film (PAF), soaking the as-prepared PAF in a targeted lubricant for swelling and erecting SLIPS to remove the redundant lubricant (Figure 1a). First, a superhydrophobic PAF with a water contact angle (WCA) of ~150° could be readily harvested by one-step femtosecond laser cross-scanning, where the width (w), length (l), and height (h) of a single micropillar and the distance (d) between isolated micropillars were characterized as 49, 46, 100, and 45 μm (Figure 1b,c), respectively. Given a further observation via high magnification, the resultant PAF is composed of a variety of laser-induced composite micro- and nanostructures including micro/nanoparticles and micro/nanoporous and isolated micropillars, which should contribute to protecting the loss of the infused lubricant oil and preventing the intrusion of the manipulated immiscible liquids (Figure S1). Compared to the previous method, femtosecond laser having the advantages of an ultrahigh manufacturing speed and an ultralow heat effect is far more efficient in altering the material's wettability by inducing hierarchical micro- and nanostructures without changing their intrinsic crystalline phase (Figure S2, Supporting Information).[28−35] Though laser fabrication is still comparatively consumptive, the cost of this high-tech manufacturing is further lowered in a manner of scalable production as the fast development with respect to

DOI: 10.1021/acs.langmuir.9b02068
Langmuir 2019, 35, 13915−13922

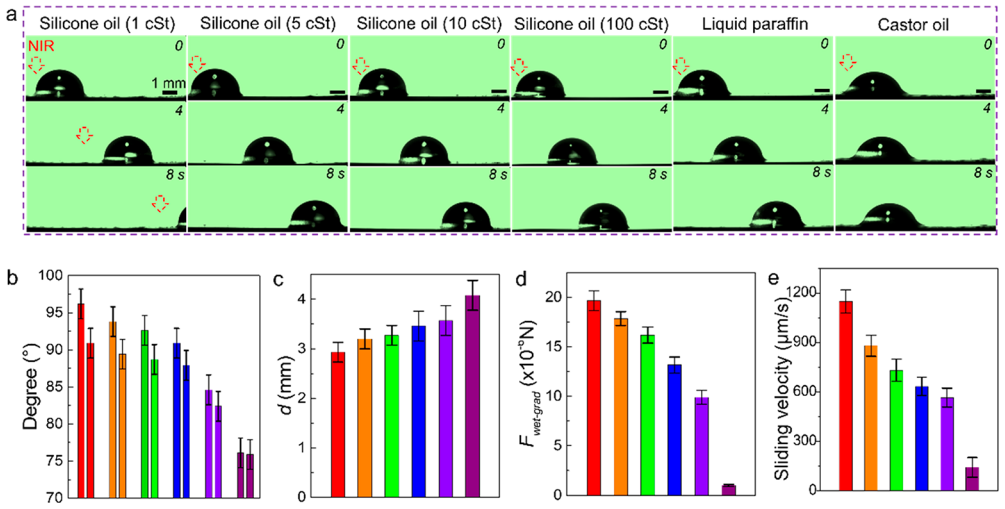

Figure 3. Influence of lubricant rheological performance on droplet motion. (a) Dynamic clips for an NIR-actuating water droplet (10 μL) sliding on six different Fe_3O_4-doped SLIPS (Fe_3O_4-doped content: 5 wt %). Corresponding numerical variations of an NIR-actuating droplet's (b) θ_A and θ_R, (c) characteristic length, (d) $F_{wet-grad}$, and (e) average sliding velocity with the increase in lubricant viscosity from 1 to 5, 10, 100, 110 and then 680 cSt, respectively.

the advanced fabrication technique. Finally, a kind of light-responsive Fe_3O_4-doped SLIPS could be harvested by infusing lubricants into the as-prepared PAF with a thickness of ~100 μm. By applying a unilateral NIR stimulus, a water micro-droplet (10 μL) could be actuated toward arbitrary directions as a function of its localized asymmetric deformation and Laplace pressure difference (P_{Lap}), which should be attributed to the temperature gradient arising from the photothermal effect of Fe_3O_4 nanoparticles (NPs) on the SLIPS (Figure 1d,e; Movie S1, Supporting Information). Typically, the localized temperature of the SLIPS was capable of increasing sharply from room temperature (RT) to 40 °C within 1 s as a result of the strong light absorption of Fe_3O_4 NPs (Figure 1f and Figure S3). As a result, the lubricant surface tension (γ_{og}) at a unilateral NIR-triggered location, which was inversely proportional to the characteristic temperature, would be decreased to elevate an apparent advancing angle (θ_A) according to the classical Young equation[36]

$$\cos\theta = (\gamma_{og} - \gamma_{ol})/\gamma_{lg}$$

where γ_{lg}, γ_{og}, and γ_{ol} represent the tensions of liquid−gas, oil−gas, and oil−liquid interfaces, respectively. Accordingly, the underlying mechanism was that a $F_{wet-grad}$, which was defined as $\gamma_{lg} \times (\cos\theta_R - \cos\theta_A) \times d$,[37] would be instantaneously generated to actuate liquid droplets in any desirable direction by modulating the NIR-irradiating sites (Figure 1g). Therein, d represents the characteristic length of a liquid droplet on the Fe_3O_4-doped SLIPS. In addition, this Fe_3O_4-doped SLIPS was capable of driving droplets for at least 50 cycles without effecting its steering performance, which indicates that this smart Nepenthes-inspired system has good stability (Figure S4).

Effect of Fe_3O_4-Doped Content on a Droplet's Hydrodynamics. Considering that the $F_{wet-grad}$ scale is mainly dominated by the difference between θ_A and θ_R for an identical droplet (10 μL, 7.2 × 10^{-2} N/m), which is determined by temperature-responsive deformation amplitude, the quantitative relationship among the weight ratio of Fe_3O_4 NPs in SLIPS, the NIR-stimulated temperature variation, $F_{wet-grad}$, and the sliding velocity should be systematically investigated. Notably, the temperature plateau for five disparate SLIPS increased from 81.6 to 96.6, 117.4, 118.5, 125.0, 123.5, and then 127.6 °C with the increase in the weight ratio of Fe_3O_4 in sequence from 1 to 7%, where its relative content was terminated at 5 wt % because no obvious increasing tendency for temperature could be reached even though we implemented a further elevation of the weight ratio (Figure 2a). Conducting a further morphology observation for droplets on five different SLIPS in the presence of a unilateral NIR stimulus, we harvested a series of experimental measurements for θ_A/θ_R and d as 91.7/89.6, 92.4/89.5, 94.2/90.3, 94.8/89.9, and 96.2/90.9° and 3.12, 3.03, 2.92, 3.00, and 2.93 mm (Figure 2b,c and Figure S5, Supporting Information), respectively. The higher the localized temperature, the smaller the γ_{og}. Therefore, the greater the relative content of Fe_3O_4, the larger the θ_A. Accordingly, the corresponding $F_{wet-grad}$ for droplets on five SLIPS were quantitatively calculated as 8.31, 11.15, 14.44, 18.63, and 19.66 (×10^{-6}) N (Figure 2d), respectively. In this view, the higher the relative content of Fe_3O_4, the larger the driving force of $F_{wet-grad}$. In addition, the average sliding velocity for droplets on five SLIPS were experimentally obtained as 235, 339, 781, 960, and 1150 μm/s, respectively (Figure 2d). The results revealed that in the initial stage the droplet hydrokinetics is highly affected by the elevation of localized temperature derived from the increased relative content of Fe_3O_4 in SLIPS, whereas it would display a saturation state with further increasing doped content up to 4 wt %. In addition to θ_A/θ_R, the influence of droplet volume, which dominates the characteristic length (l), had also been investigated by quantitative hydrokinetics analysis (Figure S6, Supporting Information). The results show that the larger the droplet size, the smaller the sliding velocity. Moreover, adjusting the irradiation height of NIR also gives rise to the change in droplet motion (Figure S7, Supporting Information). In fact, in this NIR-actuating droplet moving process, another force derived from the Marangoni effect also contributes to its moving behavior due to the surface tension gradient between the hot side and cold side of the droplet.[38] Nevertheless, the Marangoni force is far smaller than a dominant $F_{wet-grad}$ up to 1 order of magnitude,[18,26,39] so we neglected this feeble force in

DOI: 10.1021/acs.langmuir.9b02068
Langmuir 2019, 35, 13915−13922

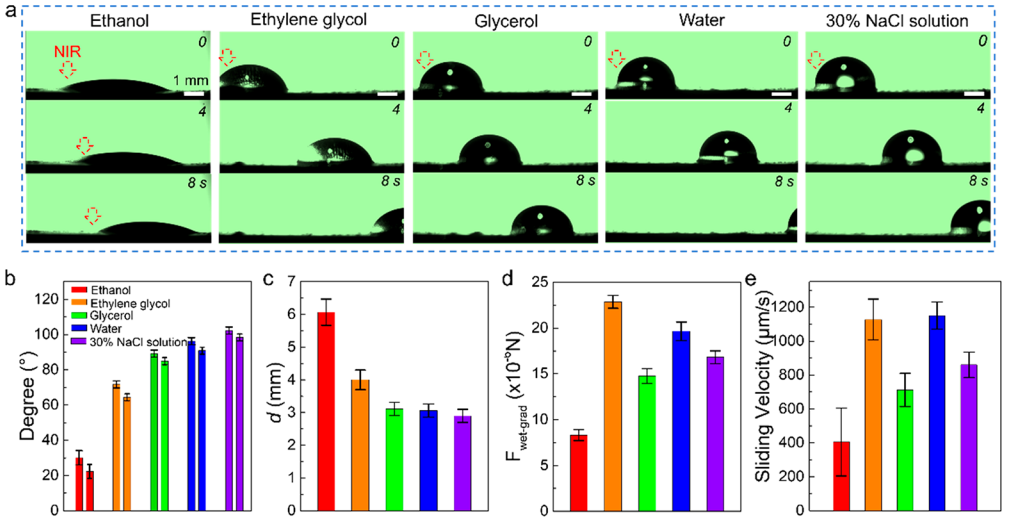

Figure 4. Manipulating diverse liquid species by Fe_3O_4-doped SLIPS. (a) Captured digital pictures for NIR-actuating ethanol, ethylene glycol, glycerol, water, and 30% NaCl droplets sliding on SLIPS (Fe_3O_4-doped content: 5 wt %). Corresponding numerical changes of an NIR-actuating droplet's (b) θ_A and θ_R, (c) characteristic length, (d) $F_{wet\text{-}grad}$, and (e) average sliding velocity for five microdroplets (10 μL).

the following investigations. (Detailed discussions can be seen in Figure S8, Supporting Information.)

Influence of Lubricant Rheological Performance on Droplet's Motion Control. The effect of lubricant rheological parameters including surface tension (γ_{og}) and viscosity (η_{og}) on a droplet's hydrokinetics should be implemented, where the former contributes to the droplet's wettability behavior and the latter, which is also defined as the hydrodynamic resistance (F_H), accounts for viscous forces in the droplet and the wetting ridge around the base of the droplet on oil-infused surfaces.[40] Accordingly, six as-prepared SLIPS with lubricants (η_{og}/γ_{og}) of silicone oil (1/1.74, 5/1.97, 10/2.01 and 100/2.1), liquid paraffin (110/3.45), and castor oil (680 cSt/3.54 ($\times$ 10^{-2}) N/m) were employed for the investigation of the droplet morphology deformation and sliding velocity variation (Figure 3a, Movie S2, Supporting Information). Seen from a sequence of captured clips, we could harvest θ_A/θ_R and d assigned to six disparate SLIPS that were measured as 96.2/90.9, 93.8/89.4, 92.6/88.7, 90.9/87.9, 84.6/82.4, and 76.1/75.9° and 2.93, 3.20, 3.27, 3.46, 3.57, and 4.08 mm (Figure 3b,c), respectively. Obviously, θ_A/θ_R decrease in contrary to the increase of d with the elevation of lubricant surface tension. Accordingly, $F_{wet\text{-}grad}$ acting on droplets on six different SLIPS were calculated as 19.66, 17.85, 16.18, 13.17, 9.90, and 1.00 ($\times 10^{-6}$) N (Figure 3d). In addition, the average velocities for NIR-actuating droplets moving on six different SLIPS, which was statistic from part (a), were calculated as 1150, 881, 732, 634, 566, and 144 μm/s, respectively (Figure 3e). The larger the lubricant viscosity, the smaller the droplet's moving velocity. The result agrees very well with a theoretical relationship between F_H and η_{og}, which could be expressed by an empirical formula[41]

$$F_H \approx \alpha(\eta_{lg} + \eta_{og})\nu\pi\frac{d}{2}$$

where α is a numerical factor, η_{lg} is the viscosity of a liquid droplet, η_{og} is the viscosity of lubricant oil, and ν is the sliding velocity of a liquid droplet. According to this empirical equation, the mechanism for the lubricant's species determining the steering performance of a liquid's transport could be revealed. The larger the lubricant viscosity, the larger the bubble sliding resistance. As a result, the lubricant viscosity can determine the droplet sliding velocity through affecting the hydrodynamic resistance. With regard to the hydrokinetic analysis of an NIR-actuated droplet moving on SLIPS, we can roughly infer that during the initial stage of light-induced motion of the droplet, $F_{wet\text{-}grad} > F_H$, the droplet would accelerate. When $F_{wet\text{-}grad} = F_H$, the droplet moves with a steady velocity. The droplet did not immediately stop even though NIR stimuli had been discharged because of the slow heat-transfer and heat-conversion process leading to a survival temperature gradient and the droplet decelerating when $F_{wet\text{-}grad} < F_H$. Until the vanishing of the residual temperature gradient, $F_H = 0$, the droplet would pin on SLIPS without NIR interference.

Manipulating Diverse Liquid Droplets by Smart SLIPS. A versatile liquid motion manipulator should be capable of steering diverse microdroplets in addition to a conventional water droplet, which is highly desirable for practical applications in lab-on-a-chip, microfluidic reactors, long-range liquid transportation, and so on.[27,42,43] To the best of our knowledge, the prerequisite for manipulating liquid droplets by a slippery lubricant-infused porous surface (SLIPS) is that the manipulated target should be immiscible with the underlying lubricant oil. On this basis, the current SLIPS demonstrated the ability of manipulating diverse droplets including ethanol, ethylene glycol, glycerol, water, and 30% NaCl aqueous solution (Figure 4a, Movie S3, Supporting Information). With the increase in the droplet's surface tension from 2.28 $\times$ 10^{-2} to 4.84 $\times$ 10^{-2}, 6.33 $\times$ 10^{-2}, 7.27 $\times$ 10^{-2}, and 8.66 $\times$ 10^{-2} N/m, θ_A/θ_R increased from 30.1/22.3 to 71.7/64.4, 89.2/84.9, 96.2/90.9, and 102.3°/98.4° (Figure 4b), respectively. The characteristic lengths for these droplets were measured to be 6.07, 4.00, 3.11, 2.93, and 2.90 mm (Figure 4c), respectively. The smaller the droplet's surface tension, the larger the droplet wetting area. Accordingly, the $F_{wet\text{-}grad}$ values for five different droplets on SLIPS were in sequence, calculated to be 8.31 $\times$ 10^{-6}, 22.86 $\times$ 10^{-6}, 14.75 $\times$ 10^{-6}, 19.66 $\times$ 10^{-6}, and 16.81 $\times$ 10^{-6} N (Figure 4d). The sliding velocity for five different droplets indicated from part a were 405, 1127, 712, 1150, and 860 μm/s, respectively (Figure 4e).

DOI: 10.1021/acs.langmuir.9b02068
Langmuir 2019, 35, 13915−13922

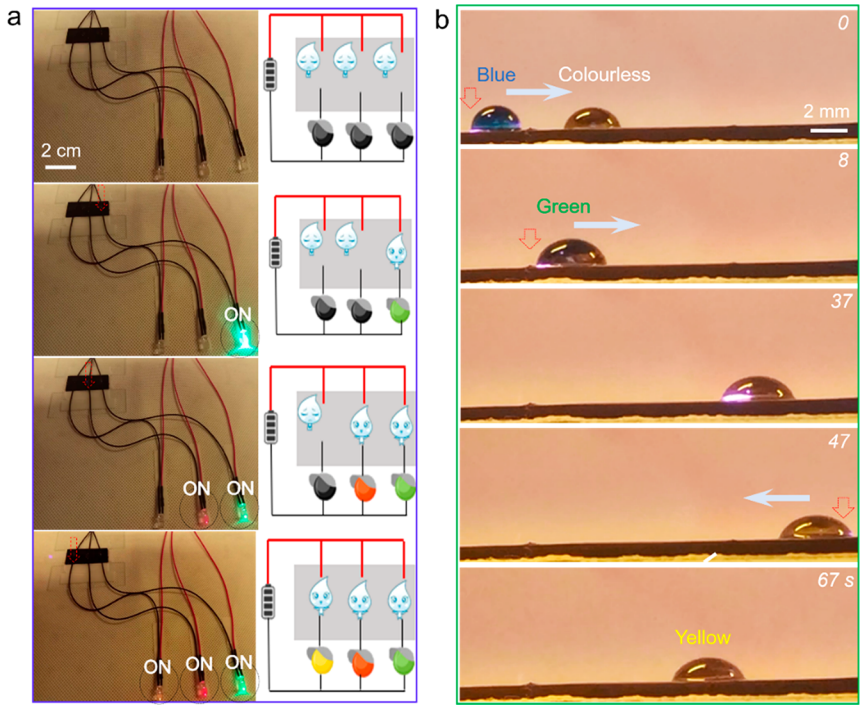

Figure 5. Programmable sliding routes for liquid droplet using Fe_3O_4-doped SLIPS. (a) Actuating conductive NaCl droplets on SLIPS to selectively lighten the traffic light. (b) Steering a blue droplet (5 μL, mixture of glucose and indigo carmine) to coalesce with a colorless NaOH droplet (5 μL) for a hybrid droplet. The result shows that the coalesced droplet is green in an initial stage and then a yellow after tens of seconds.

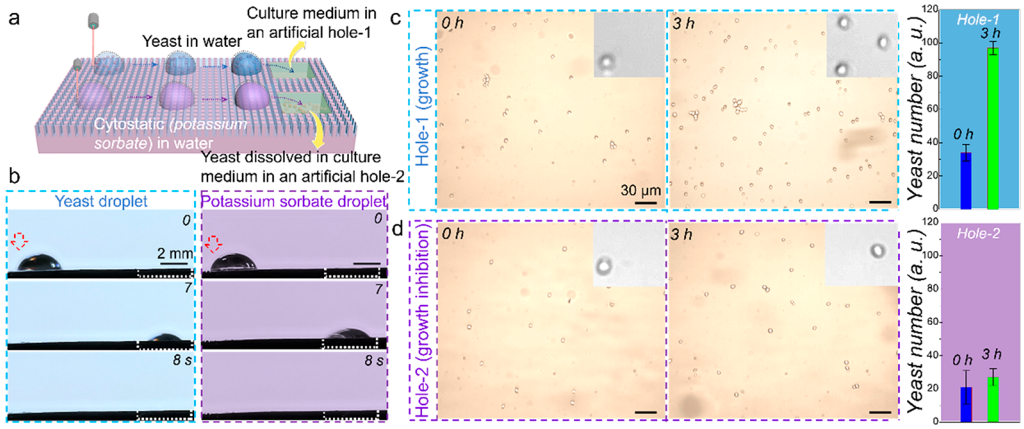

Figure 6. Biological applications of current light-responsive SLIPS. (a) Schematic diagram and (b) captured digital pictures for remotely manipulating microdroplets of biological yeast toward a targeted culture medium (hole 1) and potassium sorbate toward an as-prepared reservoir with yeast living in the culture medium (hole 2) by an NIR trigger. Captured microscopic clips for observing the growth rate of yeast in (c) hole 1 and (d) hole 2, respectively. The insets are their enlarged microscopic images for investigating cell differentiation and evolution. The right histograms are comparisons of the statistical growth rate for biological yeast cells in hole 1 and hole 2. The results show that the current light-responsive SLIPS is highly biocompatible.

In this view, the hydrokinetics of diverse liquid droplets could be readily achieved by applying a unilateral NIR stimulus.

Controllable Sliding Routes for Liquid Droplet Using Smart SLIPS. Compared to previous SLIPS, the current light-responsive SLIPS is highly competent at actuating microliquids toward arbitrary intentional routes and thus has potential applications in microfluidics on the horizontal surface, in addition to an inclined one (Figure S9, Movie S4, Supporting Information).[19,44] Here, we demonstrate its applications in controlling electrical circuits, microfluidic reactors, and the culture/inhibition of biological cells. As shown in Figure 5a, traffic lights could be selectively lightened by steering NaCl microdroplets (6 μL) toward three individual connectors (Movie S5, Supporting Information). Figure 5b displays metachromatism by steering a blue droplet (5 μL, pipetted from the as-prepared mixture of glucose and indigo carmine) and a colorless NaOH droplet (5 μL) to merge into a hybrid droplet. In the initial stage, the coalesced droplet presented a green color and then a yellow one once it had been allowed to fully react for several seconds (Movie S6, Supporting Information). Moreover, the current light-triggered SLIPS is also adaptive for biological cell manipulations without damage, and the experimental design could be observed in Figure 6a. We are capable of steering a yeast microdroplet toward a targeted artificial culture medium (hole 1) for developing cells and driving a potassium sorbate microdroplet toward a yeast

DOI: 10.1021/acs.langmuir.9b02068
Langmuir 2019, 35, 13915−13922

reservoir (hole 2) to inhibit cells by virtue of a unilateral NIR trigger (Figure 6b). The growth rate for biological yeast cells developed in hole 1 reached 285% comparing to those in hole 2 of 128%, which shows that the current light-driving method is biocompatible (Figure 6c,d).

CONCLUSIONS

We have facilely fabricated a kind of Fe_3O_4-doped SLIPS by one-step femtosecond laser cross-scanning, which can easily manipulate diverse liquids in arbitrary directions by a unilateral NIR stimulus. Upon the induced asymmetric temperature difference and $F_{wet\text{-}grad}$, we can selectively stick and slide a drop on this light-responsive SLIPS by simply loading and discharging a unilateral NIR trigger. Through modulating the NIR sites, we can slide a targeted droplet with controllable directions and routes. On the basis of the fundamental physics, we quantitatively analyzed the relationship among Fe_3O_4-doped content, lubricant rheological performance, droplet wettability variations, $F_{wet\text{-}grad}$, and the sliding velocity for diverse liquid species. Finally, we remotely manipulated liquid droplets to control the electrical circuit's switch, the microfluidic reactor, and the growth of biological cells. The current work provides guidance over the design of a stimuli-responsive slippery surface for droplet manipulation and further applications in lab-on-a-chip, microfluidics, and microengine applications.

ASSOCIATED CONTENT

Supporting Information

The Supporting Information is available free of charge on the ACS Publications website at DOI: 10.1021/acs.langmuir.9b02068.

XRD spectra; optical images of droplet motion affected by Fe_3O_4 content; quantitative hydrokinetics analysis of droplet motion influenced by volumes; the variation of velocity with different irradiating distances; and digital images of uphill motion (PDF)

Free control of a drop's motion by regulating the NIR irradiating sites (MP4)

NIR-triggered drop's motion on various lubricant-infused SLIPS (MP4)

Manipulating diverse droplets by light-responsive SLIPS (MP4)

NIR-actuating droplets' antigravity motion on inclined SLIPS (MP4)

Actuating NaCl droplets to selectively lighten traffic lights (MP4)

Steering glucose mixed droplet to coalesce with NaOH droplets for metachromatism (MP4)

Durability test for the light-responsive SLIPS (MP4)

AUTHOR INFORMATION

Corresponding Authors

*E-mail: chaoc11@ustc.edu.cn.

*E-mail: dongwu@ustc.edu.cn.

ORCID

Jiawen Li: 0000-0003-3950-6212

Yanlei Hu: 0000-0003-1964-0043

Dong Wu: 0000-0003-0623-1515

Notes

The authors declare no competing financial interest.

ACKNOWLEDGMENTS

This work was supported by the Key Project of Equipment Pre-research Field Fund in China (Grant no. 61409230310), the National Natural Science Foundation of China (nos. 51875160, 51805508, 61505047, 51875544, and 61805230), Fundamental Research Funds for the Central Universities (no. WK2090090024), and the China Postdoctoral Science Foundation (no. BH2090000025).

REFERENCES

(1) Jebrail, M. J.; Bartsch, M. S.; Patel, K. D. Digital Microfluidics: A Versatile Tool for Applications in Chemistry, Biology and Medicine. *Lab Chip* **2012**, *12*, 2452−2463.

(2) Cui, Y.; Li, D.; Bai, H. Bioinspired Smart Materials for Directional Liquid Transport. *Ind. Eng. Chem. Res.* **2017**, *56*, 4887−4897.

(3) Tang, X.; Wang, L. Loss-Free Photo-Manipulation of Droplets by Pyroelectro-Trapping on Superhydrophobic Surfaces. *ACS Nano* **2018**, *12*, 8994−9004.

(4) Park, S.-Y.; Teitell, M. A.; Chiou, E. P. Y. Single-Sided Continuous Optoelectrowetting (SCOEW) for Droplet Manipulation with Light Patterns. *Lab Chip* **2010**, *10*, 1655−1661.

(5) Su, X.; Li, H.; Lai, X.; Zhang, L.; Liao, X.; Wang, J.; Chen, Z.; He, J.; Zeng, X. Dual-Functional Superhydrophobic Textiles with Asymmetric Roll-Down/Pinned States for Water Droplet Transportation and Oil-Water Separation. *ACS Appl. Mater. Interfaces* **2018**, *10*, 4213−4221.

(6) Mi, H.-Y.; Jing, X.; Xie, H.; Huang, H.-X.; Turng, L.-S. Magnetically Driven Superhydrophobic Silica Sponge Decorated with Hierarchical Cobalt Nanoparticles for Selective Oil Absorption and Oil/Water Separation. *Chem. Eng. J.* **2018**, *337*, 541−551.

(7) Hu, S.-W.; Xu, B.-Y.; Ye, W.-K.; Xia, X.-H.; Chen, H.-Y.; Xu, J.-J. Versatile Microfluidic Droplets Array for Bioanalysis. *ACS Appl. Mater. Interfaces* **2015**, *7*, 935−940.

(8) Bruchmann, J.; Pini, I.; Gill, T. S.; Schwartz, T.; Levkin, P. A. Patterned SLIPS for the Formation of Arrays of Biofilm Microclusters with Defined Geometries. *Adv. Healthcare Mater.* **2017**, *6*, 1601082.

(9) Shahsavan, H.; Salili, S. M.; Jákli, A.; Zhao, B. Smart Muscle-Driven Self-Cleaning of Biomimetic Microstructures from Liquid Crystal Elastomers. *Adv. Mater.* **2015**, *27*, 6828−6833.

(10) Che, P.; Heng, L.; Jiang, L. Lubricant-Infused Anisotropic Porous Surface Design of Reduced Graphene Oxide Toward Electrically Driven Smart Control of Conductive Droplets' Motion. *Adv. Funct. Mater.* **2017**, *27*, 1606199.

(11) Latthe, S. S.; Sutar, R. S.; Kodag, V. S.; Bhosale, A. K.; Kumar, A. M.; Sadasivuni, K. K.; Xing, R.; Liu, S. Self − Cleaning Superhydrophobic Coatings: Potential Industrial Applications. *Prog. Org. Coat.* **2019**, *128*, 52−58.

(12) Li, N.; Wu, L.; Yu, C.; Dai, H.; Wang, T.; Dong, Z.; Jiang, L. Ballistic Jumping Drops on Superhydrophobic Surfaces via Electrostatic Manipulation. *Adv. Mater.* **2018**, *30*, 1703838.

(13) Irajizad, P.; Al-Bayati, A.; Eslami, B.; Shafquat, T.; Nazari, M.; Jafari, P.; Kashyap, V.; Masoidi, A.; Araya, D.; Ghasemi, H. Stress-Localized Durable Icephobic Surfaces. *Mater. Horiz.* **2019**, *6*, 758−766.

(14) Zhao, H.; Sun, Q.; Deng, X.; Cui, J. Earthworm-Inspired Rough Polymer Coatings with Self-Replenishing Lubrication for Adaptive Friction-Reduction and Antifouling Surfaces. *Adv. Mater.* **2018**, *30*, 1802141.

(15) Park, J. K.; Yang, Z.; Kim, S. Black Silicon/Elastomer Composite Surface with Switchable Wettability and Adhesion between Lotus and Rose Petal Effects by Mechanical Strain. *ACS Appl. Mater. Interfaces* **2017**, *9*, 33333−33340.

(16) Perez-Toralla, K.; Konda, A.; Bowen, J. J.; Jennings, E. E.; Argyropoulos, C.; Morin, S. A. Rational Synthesis of Large-Area Periodic Chemical Gradients for the Manipulation of Liquid Droplets and Gas Bubbles. *Adv. Funct. Mater.* **2018**, *28*, 1705564.

DOI: 10.1021/acs.langmuir.9b02068
Langmuir 2019, 35, 13915−13922

(17) Nichols, M. K.; Kumar, R. K.; Bassindale, P. G.; Tian, L.; Barnes, A. C.; Drinkwater, B. W.; Patil, A. J.; Mann, S. Fabrication of Micropatterned Dipeptide Hydrogels by Acoustic Trapping of Stimulus-Responsive Coacervate Droplets. *Small* **2018**, *14*, 1800739.
(18) Banuprasad, T. N.; Vinay, T. V.; Subash, C. K.; Varghese, S.; George, S. D.; Varanakkottu, S. N. Fast Transport of Water Droplets over a Thermo-Switchable Surface Using Rewritable Wettability Gradient. *ACS Appl. Mater. Interfaces* **2017**, *9*, 28046−28054.
(19) Wang, J.; Huang, Y.; You, K.; Yang, X.; Song, Y.; Zhu, H.; Xia, F.; Jiang, L. Temperature-Driven Precise Control of Biological Droplet's Adhesion on a Slippery Surface. *ACS Appl. Mater. Interfaces* **2019**, *11*, 7591−7599.
(20) Guo, T.; Che, P.; Heng, L.; Fan, L.; Jiang, L. Anisotropic Slippery Surfaces: Electric-Driven Smart Control of a Drop's Slide. *Adv. Mater.* **2016**, *28*, 6999−7007.
(21) Zhang, Y.; Zhu, B.; Liu, Y.; Wittstock, G. Hydrodynamic Dispensing and Electrical Manipulation of Attolitre Droplets. *Nat. Commun.* **2016**, *7*, 12424.
(22) Tian, D.; Zhang, N.; Zheng, X.; Hou, G.; Tian, Y.; Du, Y.; Jiang, L.; Dou, S. X. Fast Responsive and Controllable Liquid Transport on a Magnetic Fluid/Nanoarray Composite Interface. *ACS Nano* **2016**, *10*, 6220−6226.
(23) Guo, P.; Wang, Z.; Heng, L.; Zhang, Y.; Wang, X.; Jiang, L. Magnetocontrollable Droplet and Bubble Manipulation on a Stable Amphibious Slippery Gel Surface. *Adv. Funct. Mater.* **2019**, *29*, 1808717.
(24) Kwon, G.; Panchanathan, D.; Mahmoudi, S. R.; Gondal, M. A.; Mckinley, G. H.; Varanasi, K. K. Visible Light Guided Manipulation of Liquid Wettability on Photoresponsive Surfaces. *Nat. Commun.* **2017**, *8*, 14968.
(25) Ichimura, K.; Oh, S.-K.; Nakagawa, M. Light-Driven Motion of Liquids on a Photoresponsive Surface. *Science* **2000**, *288*, 1624−1626.
(26) Gao, C.; Wang, L.; Lin, Y.; Li, J.; Liu, Y.; Li, X.; Feng, S.; Zheng, Y. Droplets Manipulated on Photothermal Organogel Surfaces. *Adv. Funct. Mater.* **2018**, *28*, 1803072.
(27) Wang, J.; Gao, W.; Zhang, H.; Zou, M.; Chen, Y.; Zhao, Y. Programmable Wettability on Photocontrolled Graphene Film. *Sci. Adv.* **2018**, *4*, No. eaat7392.
(28) Yin, K.; Yang, S.; Dong, X.; Chu, D.; Duan, J.-A.; He, J. Robust Laser-Structured Asymmetrical PTFE Mesh for Underwater Directional Transportation and Continuous Collection of Gas Bubbles. *Appl. Phys. Lett.* **2018**, *112*, 243701.
(29) Yang, S.; Yin, K.; Chu, D.; He, J.; Duan, J.-A. Femtosecond Laser Structuring of Janus Foam: Water Spontaneous Antigravity Unidirectional Penetration and Pumping. *Appl. Phys. Lett.* **2018**, *113*, 203701.
(30) Duan, J.-A.; Dong, X.; Yin, K.; Yang, S.; Chu, D. A Hierarchical Superaerophilic Cone: Robust Spontaneous and Directional Transport of Gas Bubbles. *Appl. Phys. Lett.* **2018**, *113*, 203704.
(31) Yin, K.; Chu, D.; Dong, X.; Wang, C.; Duan, J.-A.; He, J. Femtosecond Laser Induced Robust Periodic Nanoripple Structured Mesh for Highly Efficient Oil-Water Separation. *Nanoscale* **2017**, *9*, 14229−14235.
(32) Yin, K.; Du, H.; Dong, X.; Wang, C.; Duan, J.-A.; He, J. A Simple Way to Achieve Bioinspired Hybrid Wettability Surface With Micro/Nanopatterns for Efficient Fog Collection. *Nanoscale* **2017**, *9*, 14620−14626.
(33) Xu, Z.; Shen, C.; Hou, Y.; Gao, H.; Sun, S. Oleylamine as Both Reducing Agent and Stabilizer in a Facile Synthesis of Magnetite Nanoparticles. *Chem. Mater.* **2009**, *21*, 1778−1780.
(34) Vorobyev, A. Y.; Guo, C. Direct Femtosecond Laser Surface Nano/Microstructuring and Its Applications. *Laser Photon. Rev.* **2013**, *7*, 385−407.
(35) Keller, U. Recent Developments in Compact Ultrafast Lasers. *Nature* **2003**, *424*, 831−838.
(36) Good, R. J. A Thermodynamic Derivation of Wenzel's Modification of Young's Equation for Contact Angles; Together with a Theory of Hysteresis. *J. Am. Chem. Soc.* **1952**, *74*, 5041−5042.
(37) Chaudhury, M. K.; Whitesides, G. M. How to Make Water Run Uphill. *Science* **1992**, *256*, 1539−1541.
(38) Irajizad, P.; Ray, S.; Farokhnia, N.; Hasnain, M.; Baldelli, S.; Ghasemi, H. Remote Droplet Manipulation on Self-Healing Thermally Activated Magnetic Slippery Surfaces. *Adv. Mater. Interfaces* **2017**, *24*, 1700009.
(39) Hou, Y.; Xue, B.; Guan, S.; Feng, S.; Geng, Z.; Sui, X.; Lu, J.; Gao, L.; Jiang, L. Temperature-Controlled Directional Spreading of Water on a Surface with High Hysteresis. *NPG Asia Mater.* **2013**, *5*, No. e77.
(40) Smith, J. D.; Dhiman, R.; Anand, S.; Reza-Garduno, E.; Cohen, R. E.; McKinley, G. H.; Varanasi, K. K. Droplet Mobility on Lubricant-Impregnated Surfaces. *Soft Matter* **2013**, *9*, 1772−1780.
(41) Bjelobrk, N.; Girard, H.-L.; Subramanyam, S. B.; Kwon, H.-M.; Quéré, D.; Varanasi, K. K. Thermocapillary Motion on Lubricant-Impregnated Surfaces. *Phys. Rev. Fluids* **2016**, *1*, 063902.
(42) Yao, X.; Hu, Y.; Grinthal, A.; Wong, T.-S.; Mahadevan, L.; Aizenberg, J. Adaptive Fluid-Infused Porous Films with Tunable Transparency and Wettability. *Nat. Mater.* **2013**, *12*, 529−534.
(43) Chen, H.; Zhang, P.; Zhang, L.; Liu, H.; Jiang, Y.; Zhang, D.; Han, Z.; Jiang, L. Continuous Directional Water Transport on the Peristome Surface of Nepenthes Alata. *Nature* **2016**, *532*, 85−89.
(44) Rao, Q.; Li, A.; Zhang, J.; Jiang, J.; Zhang, Q.; Zhan, X.; Chen, F. Multi-Functional Fluorinated Ionic Liquid Infused Slippery Surfaces with Dual-Responsive Wettability Switching and Self-Repairing. *J. Mater. Chem. A* **2019**, *7*, 2172−2183.

DOI: 10.1021/acs.langmuir.9b02068
Langmuir 2019, 35, 13915−13922